Unraveling the Dirac fermion dynamics of the bulk-insulating topological system Bi_{2}Te_{2}Se

E. Papalazarou, L. Khalil, M. Caputo, L. Perfetti, N. Nilforoushan, H. Deng, Z. Chen, S. Zhao, A. Taleb-Ibrahimi, M. Konczykowski, A. Hruban, A. Wołoś, A. Materna, L. Krusin-Elbaum, and M. Marsi

Phys. Rev. Materials **2**, 104202 — Published 3 October 2018

DOI: 10.1103/PhysRevMaterials.2.104202

Unraveling the Dirac fermion dynamics of the bulk-insulating topological system Bi_2Te_2Se

E. Papalazarou,[1,*] L. Khalil,[1,2] M. Caputo,[1] L. Perfetti,[3] N. Nilforoushan,[1] H. Deng,[4] Z. Chen,[4] S. Zhao,[4] A. Taleb-Ibrahimi,[2] M. Konczykowski,[3] A. Hruban,[5] A. Wołoś,[6] A. Materna,[7] L. Krusin-Elbaum,[4,8] and M. Marsi[1]

[1] *Laboratoire de Physique des Solides, CNRS-UMR 8502, Université Paris-Sud, Université Paris-Saclay, F-91405 Orsay, France*
[2] *Synchrotron SOLEIL, L'Orme des Merisiers, Saint Aubin BP 48, Gif-sur-Yvette F-91192, France*
[3] *Laboratoire des Solides Irradiés, Ecole Polytechnique, CNRS-UMR 7642, CEA, Université Paris-Saclay, F-91128 Palaiseau, France*
[4] *Department of Physics, The City College of New York, CUNY, New York, NY 10031, USA*
[5] *Institute of Physics Polish Academy of Sciences, al. Lotnikow 32/46, 02-668 Warsaw, Poland*
[6] *Faculty of Physics, University of Warsaw, 02-093 Warsaw, Poland*
[7] *Institute of Electronic Materials Technology, 01-919 Warsaw, Poland*
[8] *The Graduate Center, CUNY, New York, NY 10016, USA*

(Dated: August 13, 2018)

Using femtosecond time- and angle-resolved photoemission spectroscopy, we explore the out-of-equilibrium dynamics of surface fermions in the topological system Bi_2Te_2Se. We show that the presence of localized states from defects at the surface is one of the key material parameters undergirding the long relaxation time of photoexcited Dirac electrons lying in the projected band gap of the bulk insulating pristine compound. Doping this ternary compound with Sn substituting on Bi sites, while desirably increasing the resistivity at low temperatures decreases decay times of the excited homologous Dirac electrons. On the basis of these observations, we argue that long relaxation times can be ultimately controlled by a charge transfer to the surface.

PACS numbers: 78.47.J-,79.60.-i,73.20.-r

I. INTRODUCTION

Materials possessing two-dimensional (2D) Dirac states may revolutionize electronics and optoelectronic devices. Topological insulators (TIs) are among the top potential contenders[1–3]. Their unique properties spanning from high surface carrier mobilities to immunity to non-magnetic defects and impurities have been of intense attraction to a number of disciplines[4,5]. In many of the proposed applications involving TIs light pulses can be employed to control excited charge or spin currents. The efficiency of such devices will depend on the ability to control the lifetime and population of excited photocarriers and on the ability to manipulate charge balance between electrons and holes at and near the surface.

In sustaining these abilities, an extensive quest has been carried out for growing bulk-insulating TIs. The various defects generated during crystal growth used typically to heavily dope prototypical bismuth-based TIs such as Bi_2Se_3 and Bi_2Te_3. As a consequence, electronic transport properties are dominated by bulk carriers thus hindering electrical tuning of Dirac surface states (SSs). Various approaches have been employed to reduce bulk contribution, including impurity doping[6,7], electron-beam irradiation[8], and epitaxial growth of TI thin films[9].

The peculiar properties of Dirac fermions at the surfaces of TIs make it possible to photoinduce novel electronic configurations. The combination of pump-probe method and angle-resolve photoemission spectroscopy (ARPES), also known as time-resolved ARPES (TRARPES), has been the tool of choice for tackling the multi-faceted electron dynamics in TIs[10–17]. Among numerous contributions, the possibility to use ultrafast light pulses to create a transient state where the Dirac states present an effective chemical potential different from the bulk material[16], with electronic relaxation dynamics of technological interest (of the order of 50 ps) has also been reported. It has been shown that bulk or subsurface properties (such as band bending) can affect the relaxation dynamics of Dirac SSs. Recently, TRAPRES investigation on the bulk-insulating TI Bi_2Te_2Se (BTS) has shown to exhibit extremely long relaxation dynamics, exceeding tens of microseconds, and coexisting with a long-lived surface photovoltage (SPV)[17]. Short while ago, time-resolved experiments performed in other bulk-insulating bismuth chalcogenide TIs, namely Bi_2Te_3 and $GeBi_2Te_4$, showed long relaxation dynamics in the picosecond timescale, though without presenting SPV[18]. SmB_6, a bulk-insulating TI candidate with resistivity attaining 20 Ωcm, has also shown an exceptionally-long transient SPV with a duration exceeding 200 μs[19].

This article reports additional experimental measurements in quest to untangling the long relaxation dynamics of out-of-equilibrium fermions in bulk-insulating TIs. From this perspective, we have investigated the ternary tetradymite compound BTS (Fig. 1) alongside with its Sn-doped sibling. BTS displays high bulk resistivity (1-6 Ωcm at 4 K), turning this TI variant to be a handy material to study topological SSs without interference from bulk electronic states and hence of particular interest in novel photonic and optoelectronic applications. The high resistivity is thought to arise from the sup-

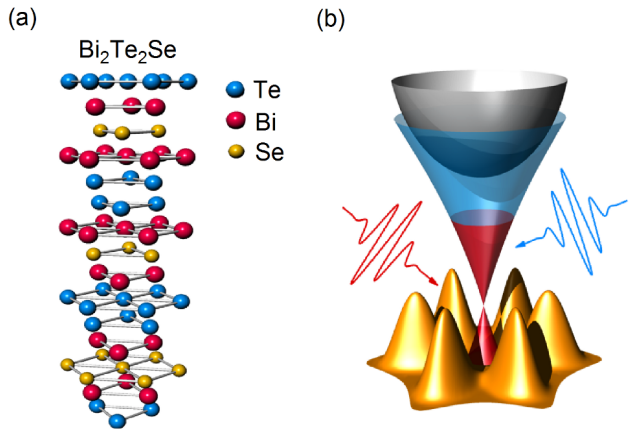

FIG. 1. (Color online) (a) Crystal structure of Bi_2Te_2Se ternary system; in the unit cell shown Bi (red), Se (yellow), and Te atoms (blue). (b) A sketch of the bandstructure where the presence of n-type Dirac fermions is indicated by red filling of the Dirac cone. Bulk holes are photoexcited (red photon) to the bulk conduction bands and their subsequent time evolution is recorded by the delayed probe (blue photon).

pression of Se vacancies, from the enhanced formation of Bi_{Te} (p-type) and Te_{Bi} (n-type) antisite defects, and from the reduced Se/Te randomness[20–22]. Since the bulk carrier concentration can be thermally controlled[20], it is possible to experimentally realize a situation where the band position at the surface is fixed by the surface pinning states, while the band position in the bulk can be independently tuned by adjusting the temperature. Our study demonstrates that the remarkably long decay times of Dirac fermions is militated by special surface defect states inducing a near-surface potential acting to separate opposite charge carriers. Further, we show that this near-surface potential (not to be confused with the long range band bending) is not responsible for the observed SPV, but is essential to hinder charge recombination in the Dirac SSs. Incorporation of Sn into BTS induces lower charge carrier concentrations and therefore higher resistivities as Sn atoms efficiently compensate the native electron donors[23]. Nevertheless, we found that Sn-doping drastically reduces the recombination time as photoexcited carriers speedily relax by enhanced impurity scattering events. Electrostatic gating experiments in these compounds are consistent with the presence of trap states which can be ultimately controlled by gate voltage and by a deliberate surface charge transfer through which band bending can be tuned[9].

II. METHOD AND EXPERIMENTAL DETAILS

We have investigated near-stoichiometric BTS and Sn(%1)-doped BTS single crystals. The crystals were grown by the standard Bridgman-Stockbarger method using a vertical temperature gradient pull. Electrical resistivity measurements were performed on 80 μm-thick, $\sim$1$\times$1 mm^2 large specimens.

The time-resolved photoemission experiments were performed in the FemtoARPES setup. A commercial Ti:sapphire laser system delivers 40 fs pulses at 1.57 eV of photon energy and at 0.25 MHz of repetition rate. Ultraviolet probe pulses of 6.3 eV are generated by cascade frequency mixing in β-BaB_2O_4 non-linear crystals. Pump and probe beams were focused almost collinearly on the sample surface[24]. In this particular experiment, we tuned the pulse duration of the ultraviolet probe pulses thus to achieve an energy resolution of $\approx$ 40 meV. The measurements were performed at a base pressure of 7×10^{-11} mbar. The spot-size of the UV probe beam at the sample's surface is $\sim$40 μm while that of the pump beam is $\sim$180 μm. The probe photon flux was adequately reduced in order to avoid a shift of spectra induced by space-charge effect, *i.e.* the spectral shift due to the effect is estimated to be less than 4 meV. The incident pump fluence was fixed at 120 ± 5 μJ/cm^2 unless explicitly stated. Thick specimens (>100 μm) from the same boule used for the transport measurements were mounted on a cryogenic manipulator and cleaved *in situ* under ultra high vacuum. Thick samples and consistent cleaving procedure assured similar resistivities after cleavage.

Ex situ transport, Shubnikov-de Haas (SdH) oscillations and gating measurements of thin crystals, were performed in Quantum Design PPMS system equipped with a 14 T magnet. A large number of back-gated devices were fabricated by exfoliation of pristine BTS single crystals to flakes of thicknesses of 100 nm and below and by placing on 90 nm thick SiO_2/Si substrates. For samples thinner than 50 nm e-beam lithography was used.

III. RESULTS AND DISCUSSION

A. Surface photovoltage and carrier dynamics in stoichiometric BTS single crystals

All the pristine BTS compounds studied here have high resistivity at low temperatures, with n-type conduction indicative of low-temperature transport dominated by surface electrons (see Appendix A for details); V-shaped magnetoresistance emerging in this n-type conductivity region exhibits a 2D scaling, thus confirming the surface origin of the conduction (see Appendix A, Fig. 8).

Figs. 2(a)-2(c) show intensity maps from pristine BTS acquired at emission angles near $\bar{\Gamma}$ for selected pump-probe delays for various temperatures. We use as energy scale the measured kinetic energies in all presented ARPES intensity maps. The figures on the very left-hand side show spectra without pump laser pulses. The Dirac point (DP) (dashed red lines) is located at 1.748 ± 0.01 eV, 1.782 ± 0.01 eV and 1.802 ± 0.01 eV, at temperatures of 40 K, 80 K and 120 K, respectively. The positions were found by fitting the energy distribution curves near $\bar{\Gamma}$ with Gaussian functions. The surface chemical

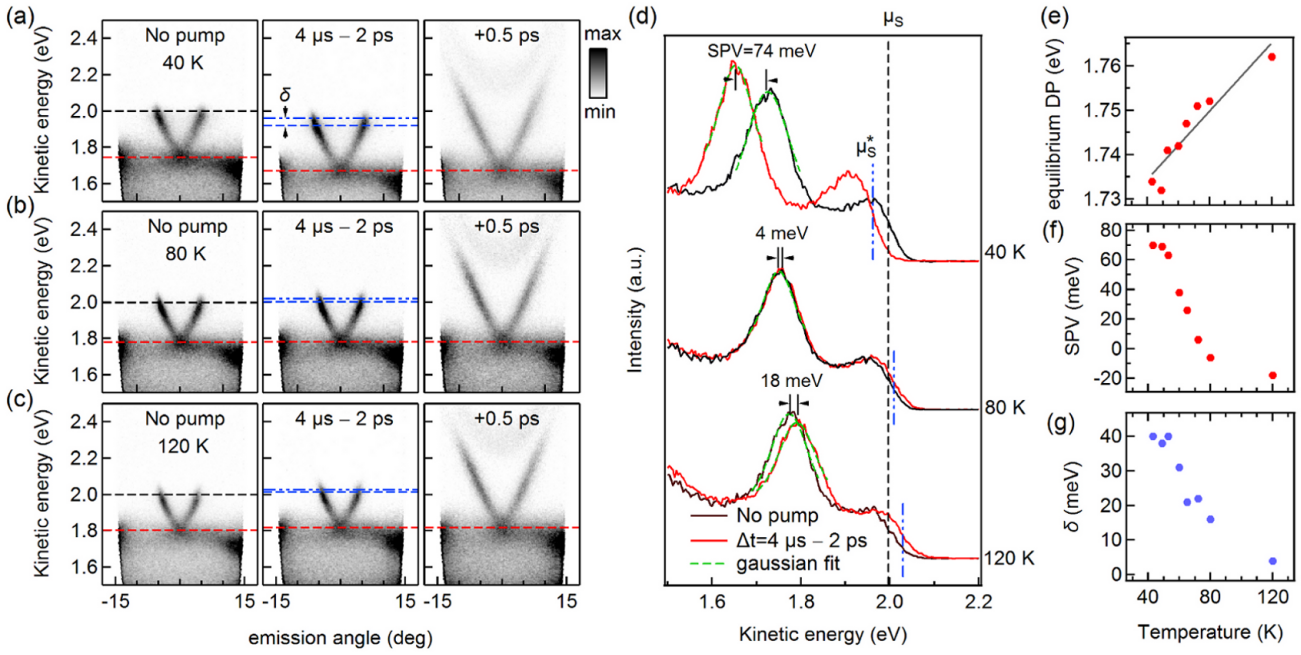

FIG. 2. (Color online) TRARPES spectra of a pristine BTS. The intensity maps have been acquired at emission angles near $\bar{\Gamma}$ for selected pump-probe delays at 40 K (a), 80 K (b) and 120 K (c). Black dashed lines, in left panel, represent the surface chemical potential, μ_S, in equilibrium (no pump) and red dashed lines the position of the DP. In mid panels, blue dashed lines show the position of the μ_S shifted by SPV, blue dash-dotted lines show the transient surface chemical potential, $\mu_S^\star$, at $\Delta t = 4$ μs-2 ps (steady state) and δ depicts the energy difference between $\mu_S^\star$ and μ_S-SPV. (d) Angle-integrated EDCs extracted from the spectra in (a), (b) and (c) without pump (black curves) and with pump at delay of $\Delta t = 4$ μs-2 ps (red curves). Green dashed curves are gaussian fits. Note that SPV changes sign from positive, at 120 K to negative, at 40 K. The energy shift at 40 K is as large as 74 meV, whereas it reduces to nearly 18 meV at 120 K. (e) The position of the DP in thermal equilibrium (the black straight line is a linear regression) and (f) the evolution of SPV amplitude acquired with a pump fluence of 120 ± 5 μJ/cm^2 at $\Delta t = 4$ μs-2 ps. (g) Evolution of δ as a function of temperature.

potential in thermal equilibrium, μ_S, is obtained by fitting the energy distribution curves (EDCs) with a Fermi-Dirac distribution function, and it turns out to be at 1.992 ± 0.01 eV. When the sample is irradiated by the pump pulse, at 40 K, the whole band structure shifts substantially downwards while at 80 K and 120 K the shift changes sign, *i.e.* bands shift upwards. We attribute this band shift to the presence of a SPV caused by the incident infrared pulses. Figure 2(d) shows angle-integrated spectra around $\bar{\Gamma}$ extracted from the intensity maps in Figs. 2(a)-2(c). We note that at 40 K, the shift can be as large as ≈74 meV. The presence of SPV is meant to be due to a pre-existing band bending when samples were cleaved in vacuum; this is in line with previous studies performed on metal-semiconductor and vacuum-semiconductor interfaces[25–28]. Indeed, surface band bending is known to be related to the existence of localized states arising from various surface and near-surface phenomena that perturb the local charge balance[29]. The surface chemical potential pinning depends on the type of these localized states (donors or acceptors) and the direction of the band bending on the type of the majority carriers. The origin of defect states in stoichiometric BTS has been discussed by several authors. It was reported that a large number of Te_{Bi} or Se_{Bi} antisite defects located in the Bi layer act as charge donors. On the other hand, BTS single crystals may hold acceptor-like impurity states (such as Bi_{Te} antisite defects and Bi vacancies) residing deeper within the energy band gap[20,30–32]. The measured bulk resistivity unveils an Arrhenius behavior for temperatures above T_0 while it nearly saturates at lower T. Such behavior is attributed to thermally activated bulk carriers in the valence or conduction band hopping from, or to, in-gap impurity states[20,32]. The effective activation energy Δ is ≈22 meV, ($T > T_0$) (see Appendix A). For $T < T_0$ the process is not thermally activated, but conduction may take place via a variable-range hopping[33]. Finally, at the surface, Te vacancies would tend to pin μ_S closer to conduction band minimum[22].

At 40 K, μ_S is pinned at 250(10) meV above the DP. With increasing temperature, DP tapers linearly towards weaker binding energies. The probed position of the DP at thermal equilibrium as a function of temperature is shown in Fig. 2(e). The origin of this behavior is discussed later.

When the sample is irradiated by the pump pulse, the DP displays a large shift due to SPV. Figure 2(f)

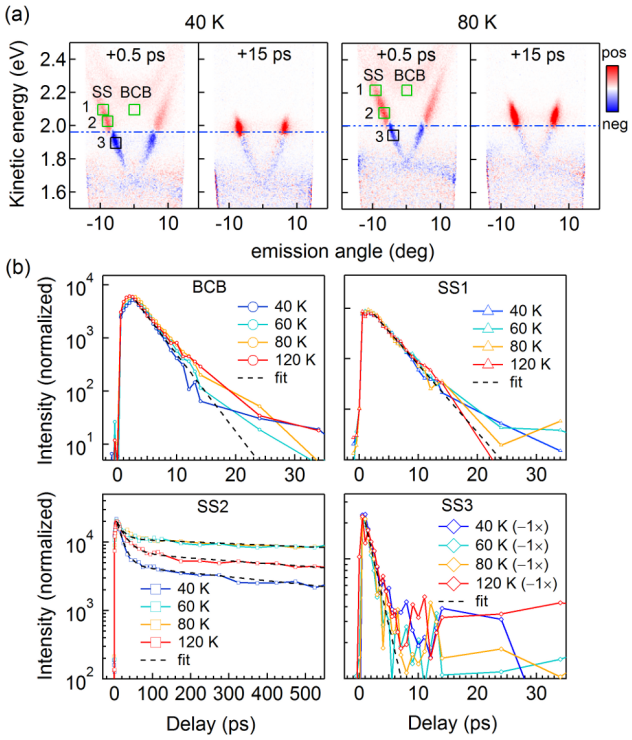

FIG. 3. (Color online) (a) Difference ARPES spectra of a pristine BTS obtained by subtracting probed spectra at delays of +0.5 ps and +15 ps from their negative counterpart at 4 μs−2 ps, at 40 K and 80 K. Blue dash-dotted lines show $\mu_S^\star$ at 4 μs−2 ps (steady state). (b) Comparison of the ultrafast temporal evolution of Dirac SSs, *i.e.* integration windows SS1, SS2 and SS3, and the bottom of BCB, *i.e.* integration window BCB, at the subsequent temperatures. A fit to exponential decay is shown as black dashed lines.

shows the evolution of the SPV amplitude as a function of temperature obtained by TRARPES intensity maps at $\Delta t = 4$ μs−2 ps. It should also be noted that at a fluence of 120 μJ/cm^2 the SPV appears to be nearly saturated (the evolution of the SPV as a function of the pump fluence is shown in the Appendix B). In our TRARPES images, we also observe that $\mu_S^\star$ at $\Delta t = 4$ μs−2 ps (obtained by fitting EDCs with a Fermi-Dirac distribution) varies with temperature. In particular, Fig. 2(g) shows the evolution of the energy difference, δ, between $\mu_S^\star$ and the μ_S−SPV as a function of temperature. At 40 K, δ is nearly 38(4) meV, whereas at 120 K it decreases down to ≈4 meV. The physical origin of this quantity emerges from surface electrons accumulated in Dirac SSs right above μ_S−SPV. This means that a transient electron population is retained in SSs for delays longer than the laser's repetition rate (also known as steady state) and this population increases with decreasing temperature. This point is discussed further in subsection B.

Next we turn to a systematic tracking of the transient population of the involved surface and bulk states as we change the sample temperature. Figure 3(a) shows difference transient ARPES intensity maps obtained by subtracting spectra at a positive delay of $\Delta t = +0.5$ ps by their negative delay counterparts (at $\Delta t = 4$ μs−2 ps). Figure 3(b) shows the respective ultrafast time evolution of Dirac-like SSs and bulk bands extracted from the selected integration windows (green boxes). The positions of the integration windows were chosen with respect to the DP. Almost immediately with the arrival of the pump pulse a strong out-of-equilibrium electronic state is built up with excess carriers populating surface and bulk states. We know from previous studies[10,15] that within the interval of a few picoseconds the various interband and intraband scattering processes involve to accumulate the excess carriers in lower lying Dirac SSs as well as in the bottom of bulk conduction band (BCB). The relaxation dynamics of these states depends on their nature and on the sample temperature. In order to establish a comparative picture on the transient population of the SSs we have chosen integration windows at a fixed energy. SS2 and SS3 windows are located ≈50 meV above and below $\mu_S^\star$. The characteristic relaxation times of BCB and SS1 are found by fitting the data with a single exponential decay function. For BCB, the decay time is $\tau_{BCB} = 3.2 \pm 0.5$ ps and for SS1, $\tau_{S1} = 3.3 \pm 0.2$ ps. Note that BCB and SS1 have similar relaxation rates[15] while they are temperature independent. However, SSs lying in the projected band gap, right below the BCB, present a slower relaxation component reflecting the presence of an energy gap in the bulk electronic states. Table I summarizes the characteristic decay times, τ_1 and τ_2, found by fitting SS2 with a double exponential decay function. Note also that, on the longer timescale, a slower dynamics falling outside of our measurement window (1 ns) lead to a steady state with $\delta > 0$ in SS2. Therefore, the complete relaxation back to the equilibrium exceeds 4 μs that is the time interval between two consecutive laser pulses. We also observe that at $T > T_0$ ($T < T_0$), μ_S pins closer to BVB (BCB). Interestingly, SSs below $\mu_S^\star$ have decay times shorter than or similar to BCB states, *i.e.* $\tau_{SS3} = 2.4 \pm 0.4$ ps. It follows that excited electrons occupy SSs (in SS2) for microseconds, whereas excited holes desert SSs (in SS3) after a few picoseconds. This can only be understood in the context of the presence of an electric field that retards the electron-hole recombination in the Dirac SSs, eventually leading to a steady state. The nature of this electric field is discussed in subsection B below.

TABLE I. Characteristic decay times of SSs in the projected band gap, SS2, as a function of temperature.

Temperature (K)	τ_1 (ps)	τ_2 (ns)
40	16 ± 1	0.7 ± 0.1
60	20 ± 3	2.1 ± 0.4
80	28 ± 3	2.1 ± 0.3
120	24 ± 1	1.1 ± 0.1

In the following, we report TRARPES results as a function of the pump fluence from 6 ± 3 μJ/cm^2 up to

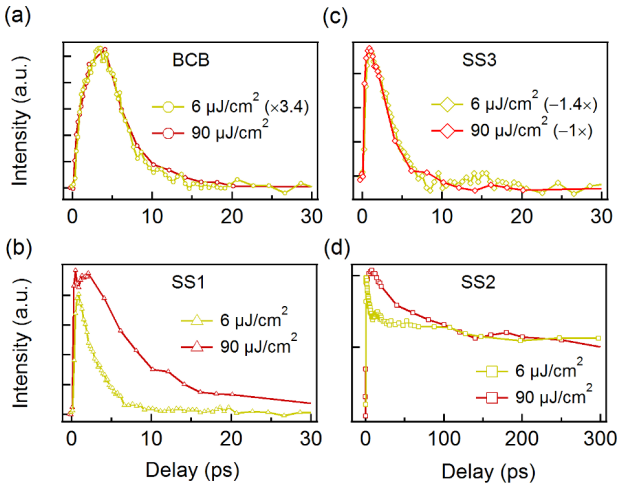

FIG. 4. (Color online) (a)-(d) Time-resolved evolution of SSs (integration windows SS1, SS2, SS3) and BCB (integration window BCB) at fluence of 6 ± 3 μJ/cm^2 and 90 ± 5 μJ/cm^2. The sample temperature was kept at 40 K.

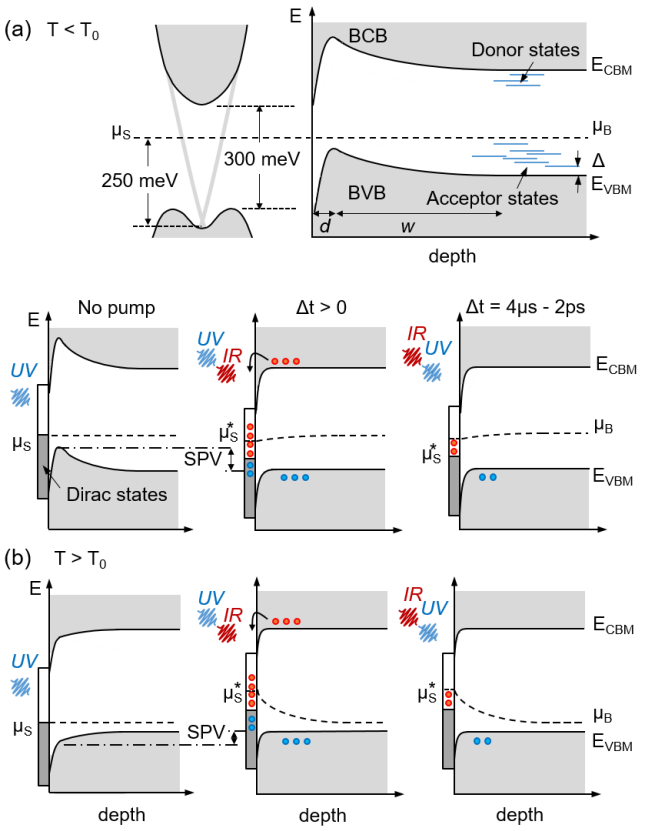

FIG. 5. (Color online) (a) Schematic energy diagrams of the electronic band structure from the surface down to the bulk for temperatures (a) below and (b) above T_0. Top and left-hand panels show diagrams at equilibrium, while mid and right-hand panels upon photo-excitation. The diagrams depict in addition to a depletion region, w, from a long-range band bending a near-surface energy shift extending over few quintuple layers, d. States below the conduction band minimum, E_{CBM}, and above the valence band maximum, E_{VBM} represent ionized and non-ionized impurities.

90 ± 5 μJ/cm^2. At 40 K, the BTS specimen has its equilibrium surface chemical potential within the bulk band gap, and thus only the Dirac SSs cross the Fermi level, which is consistent with the bulk insulating behavior observed in transport measurements (see Appendix A). Figs. 4(a)-4(d) show the time-resolved evolution of SSs and BCB. Let us first note that the electron population in BCB increases with increasing pump fluence, while the decay times are independent of it. Second, we find that the maximum value of the excess hole intensity (see SS3) is reached at about 800 fs after photo-excitation. Moreover, a closer inspection reveals that this value is weakly dependent of the pump fluence. Finally, exponential fits to SS2 (in-gap Dirac electrons) and SS3 (holes) curves reveal that even at a high pumping fluence the SS2 decay time is a few orders of magnitude greater than that of SS3. Following the timescales in SS2 curves, we argue that the phonon-assisted recombination is hindered by a spatial separation between photoexcited electrons and holes. Note also that a long-range band bending would have been flattened under high excitation fluence (>40 μJ/cm^2). The later seems being in stark contrast to the observed charge carrier separation. In the following subsection we discuss a possible mechanism that could account for this apparent contradiction.

B. Mechanism for the relaxation dynamics of surface carriers

Long relaxation dynamics of surface electrons in bulk-insulating TIs was recently discussed in various references in the literature. Among those, it was suggested that the energy dissipation of photoexcited carriers in Dirac SSs is mainly mediated by electron-phonon scattering along the surface[18]. Nevertheless, such a relaxation mechanism involves on the picosecond timescale[34].

Bismuth chalcogenide TIs are also known for being excellent thermoelectric materials. In BTS single crystals, the Seebeck coefficient has measured to be as high as 350-400 μV/K[35] at room temperature inasmuch as carrier concentrations are low and close to n-p crossover. Note that the measured values are prone to variation because of their sensitivity to the exact material composition. Nevertheless, a high Seebeck coefficient would create a substantial surface-bulk potential difference in presence of a temperature gradient created from laser pulses shining the surface. The necessary temperature gradient to shift the surface chemical potential over 40 meV would be 100 K. This constitutes a significant temperature difference and, therefore the contribution of Seebeck effect is expected being negligible under the afore mentioned pump fluences.

It has also been argued that the charge carrier separa-

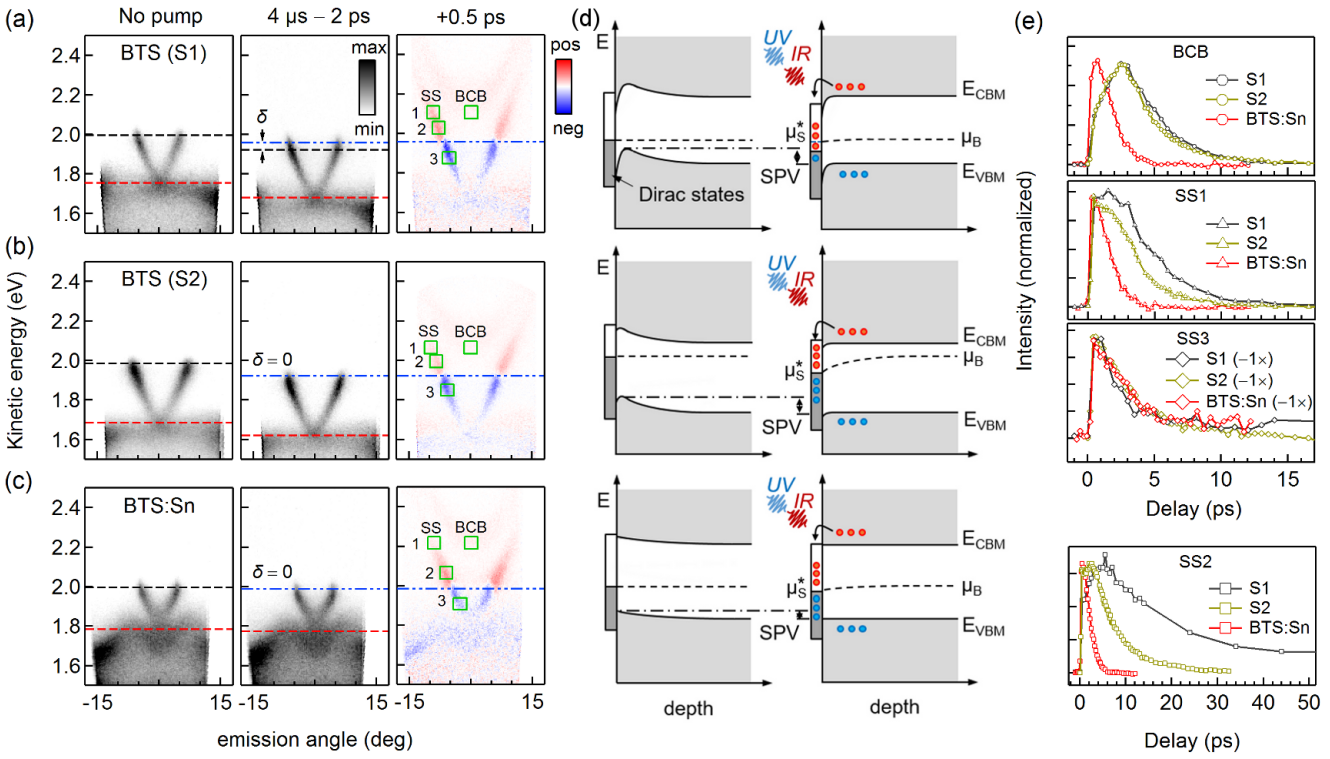

FIG. 6. (Color online) Comparison of three bulk insulating bismuth chalcogenide compounds at 40 K. *From the left to the right*: ARPES spectra without pump, at a pump-probe delay of 4 μs−2 ps and difference ARPES spectra at a pump-probe delay of +0.5 ps of (a) pristine BTS specimen 1 (S1), (b) pristine BTS specimen 2 (S2) and (c) Sn-doped BTS. (d) Schematic illustration of the respective band diagrams of the surface and depletion region as well as of the suggested upon photo-excitation relaxation mechanisms. (e) Comparison of the ultrafast evolution of the electron population of surface and bulk states for the selected integration windows in (a), (b) and (c).

tion near the surface region may be due to an emerging laser-induced band bending on femtosecond timescale[36]. Under laser-excitation of a bulk-insulating TI, excited carriers in SSs undergo an ultrafast thermalization establishing a Fermi-Dirac equilibrium. These carriers, unable to diffuse into the bulk dissipate their energy in Dirac SSs. Meanwhile, thermalized bulk carriers reach the surface on different timescales according to their effective mass and mobility (electrons diffuse faster than holes). Conforming to this diffusion mechanism, an upward photo-induced band bending would emerge regardless of the temperature. This conjecture is in clear contrast with our time-resolved data as we observed that the SPV changes sign at T_0. Moreover, the proposed photo-induced band bending should be a general property of a bulk-insulating TI. However, we show in subsection C relevant counter-exemples from similar TIs where no charge separation was observed.

It was previously reported that a pre-existing band bending may naturally account for the long charge carrier dynamics exceeding several tens of picoseconds; the built-in surface electric potential from surface traps induces a macroscopic charge carrier separation affecting substantially the relaxation dynamics of Dirac SSs[16]. We have also witnessed from fluence dependence measurements that over a certain fluence SPV reaches saturation; something that is expected when excited excess charge carriers screen the surface charge thus reducing the long-range depletion region (band flattening). Unlike this situation, Fig. 4 depicts that the asymmetry between the photoexcited electron (SS2 window) and hole density (SS3 window) is sustained even at high pump fluences. Moreover, TRARPES images around T_0 (see for instance Fig. 3) seem following a very similar trend, that is a non-zero δ. Based on these results, we infer that i) a surface electric field should be reponsible for the macroscopic charge carrier separation and that ii) the photoexcited charge density is unable to screen it.

The most plausible interpretation for our observations would be an additional downward shift of the surface band structure. The microscopic origin of this near-surface potential has been previousely discussed in the context of vacancies and adatoms on a pristine Bi_2Se_3[37,38]. Accordingly, special defects such as donor-type vacancies (e.g., V_{Te}) created on cleaved surfaces change the charge density inside the crystal within few quintuple layers (3-5 nm) constituting the key parameter for inducing a surface electrostatic potential. With this in mind, we argue that the near-surface potential acts as a potential barrier for the photoexcited holes beneath the

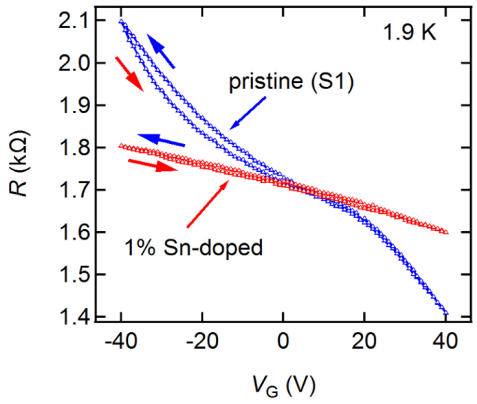

FIG. 7. (Color online) Gating hysteresis in the longitudinal sheet resistance R of a ∼30 nm thick pristine and 1% Sn-doped BTS crystals at 1.9 K.

surface (assuming ≈30 nm of penetration depth for the pump pulse[10]). We emphasize that while near-surface potential is built-up in the topmost layers, a long-range band bending is extended over a large depletion region that is w ≈75 nm at 40 K (see Appendix B). Hence, for $T < T_0$ the near-surface potential is responsible for the accumulation of electrons in the Dirac SSs and the extraordinarily long (more than 4 μs) photoexcited charge carrier relaxation time; the electron population included into δ in Fig. 2(a) at 4 μs−2 ps show a steady state situation. By the same token, for $T > T_0$ valence electrons hop to impurity states, via thermal fluctuations, thus increasing the bulk carrier population. The material becomes effectively p-type, thus inversing the local charge balance and eventually leading to a downward long-range band bending. The observed small amplitude of SPV at 120 K and the observed increase of the SSs relaxation rate are both in perfect agreement with this picture. We also argue that the observed logarithmic dependence of the SPV on the pump fluence can only be interpreted in terms of a long-range band bending as photoexcited electron-hole pairs provide the required charge to compensate the built-in electrostatic potential. On the other hand, screening a strong near-surface potential built in few quintuple layers below the surface would require higher excitation fluence. Assuming that the amplitude of the downward potential shift at the surface exceeds 22 mV (at 40 K), that is above the activation energy of acceptor impurities, the built electrostatic field will be at least 10^5 V/cm and the surface charge density over 10^{13} cm^{-2}. This constitutes a strong field to screen and, hence a significant energy barrier for thermalized carriers at the valence band maximum to surmount. In Figs. 5(a) and 5(b), we illustrate the energy diagram of the electronic band structure extending from the surface down to the bulk. In drawing it, we adopted a band gap of 300 meV and an impurity active gap of 22 meV. Assuming a band bending of ≈74 meV at 40 K, μ_B must be located well above Δ. The built depletion region, w, extends over 75 nm, while a near-surface potential manifests itself in few quintuple layers below the surface. Upon photo-excitation (mid panel), photoexcited electrons drift towards surface filling up SSs. Subsequently, a steady-state situation is reached (right-hand panel) where the charge balance of surface carriers is breached due to the presence of a potential barrier that prevents holes from reaching the surface.

Finally, we should state that the leading mechanism responsible for the near-surface potential and, hence for the charge carrier separation is *independent* of the topological nature of this compound. Therefore, it may occur in other layered semiconducting systems, e.g. in the family of transition metal dichalcogenides[39].

C. The role of impurities in the electron relaxation

We now turn our discussion to the influence of the bulk resistivity in out-of-equilibrium charge carriers relaxation times. We performed a large number of consecutive TRARPES measurements on different freshly cleaved ternary tetradymite compounds; on two pristine BTS specimens cut from different boules (labeled as S1 and S2) and a Sn-doped BTS. We call S1 the BTS specimen cut from the same boule as the one discussed above.

Figure 6 summarizes the energy-angle of emission images of the involved compounds. In Figs. 6(a)-6(c), we show ARPES images of the band structure without the pump beam, at a pump-probe delay of 4 μs−2 ps and difference spectra at +0.5 ps. At 40 K, μ_S in BTS S2 is pinned at 300(10) meV far above the DP. Owning a measured SPV of ∼80 meV, the μ_B is pinned at ∼10 meV below BCB. The resulting bulk electron concentration of $\sim 3.9 \times 10^{17}$ cm^{-3} from the measured Hall resistivity is in line with this picture. This high bulk carrier concentration at $T < T_0$ as well as for $T > T_0$ suggests higher density of impurity states than that of BTS S1. Figure 6(e) shows the comparison of the transient population of surface and bulk states for the selected integration windows in Figs. 6(a)-6(c). We note the striking difference in the relaxation times of near-Fermi SSs, *i.e.* SS2 windows: in BTS S2, photoexcited electrons in Dirac SSs relax nearly 6 orders of magnitude faster than their counterparts in BTS S1. This suggests that the amplitude of the near-surface potential in BTS S2 is not large enough to prevent holes from recombining with Dirac electrons. In BTS S1, the decrease of δ with increasing temperature indicates that holes can acquire sufficiently high thermal energy to tunnel through the barrier and reach the surface and eventually recombine with electrons in SSs.

Sn-doped BTS, on the other hand, represents still higher bulk resistivity of ≈13 Ωcm (that is over an order-of-magnitude higher than pristine BTS samples) with a conduction type conversion temperature T_0 similar to the pristine BTS samples, in the 73-80 K range (see Appendix A, Fig. 8). At 40 K, the amplitude of the SPV is

nearly 18 meV, to be compared to the 70-80 meV measured in the pristine compounds (see Appendix B for the evolution of the SPV). Analysis of the photoexcited electrons in BCB shows a nearly 3 times faster caracteristic relaxation time than of their counterparts in the pristine compounds. For SSs electrons lying in the gap this difference is more than remarkable. Recent k-dependent electronic structure calculations demonstrated that Sn impurities compensate native donors and reduce the number of Bi_{Te} antisite defects forming localized impurity states located deep into the band gap acting as charge carrier concentration buffer[23]. The higher bulk resistivity, ultimately enhances the surface transport and substiantally increases the decay rate of photoexcited fermions. The measured relaxation time of ≈10 ps is comparable to that found in other TIs from the tetradymite family, notably in a nearly stoichiometric Bi_2Se_3[12]. This compound is known for being heavily n-type owing to a large amount of charged Se vacancies[40]. Figure 6(d), illustrates the band diagrams of the surface, space-charge region and the suggested relaxation mechanisms in our photoexcited bulk insulating TI compounds.

Electrostatic gate-dependent charge transport measurements performed in ∼30 nm single crystal flakes of pristine specimens confirm the above suggested scenario (Fig. 7). In the pristine BTS compound, the measured longitudinal sheet resistance, R, displays a hysteretic behavior when the applied back-gate voltage V_G sweeps back and forth, while in the Sn-doped compound there was no detectable hysteresis (including the experimental error). Moreover, in pristine crystals hysteresis is asymmetric and does not depend on V_G sweep rate in the 0.1 to 1 V/s range (Appendix C), consistent with long relaxation seen in TRARPES. In the Sn-doped crystal, the gating sweep in the same range is symmetric and, within the experimental uncertainty, hysteresis is not detected. A non-negligible electrostatic gating hysteresis is known to result from surface traps[41]. The found gating hysteresis can be removed by cooling while under gate bias which neutralizes charge traps (see Appendix C2, Fig. 12). Thus, our findings suggest that trap states, and thus carrier relaxation times, could potentially be manipulated by gate voltage.

IV. CONCLUSION

Our systematic comparison of truly bulk insulating ternary tetradymite compounds, whose type and charge carrier concentration can be tuned with temperature, leads us to conclude that special surface defect states, along with the high quality of the crystal growth, induce a near-surface potential that accounts for the spatial separation between excess electrons in the surface and holes in the subsurface region and, hence for the long relaxation dynamics observed in Dirac SSs. Further, we showed that the observed SPV is induced by impurity states residing in the energy band gap and it can be understood in terms of a photoinduced screening of a long-range band bending. Electrostatic gating performed on both thin and thick samples confirmed our ARPES observations, implying that it could be used to tune the carrier relaxation times. Moreover, controlling the spatial separation of Dirac carriers may open up the possibility to study other exotic quantum phenomena such as the topological exciton condensate between two separated Dirac electrons and Dirac holes in a vertical p-n jonction[42]. These results should be taken into account in the engineering of semiconductor compounds for novel optical and optoelectronic devices based on topologically non-trivial SSs.

ACKNOWLEDGMENTS

The FemtoARPES activities were funded by the RTRA Triangle de la Physique, the Ecole Polytechnique, the EU/FP7 under the contract Go Fast (Grant No. 280555). M.M., L.P., M.K. M.C. and E.P. work was supported by "Investissement d'avenir Labex Palm" (Grant No. ANR-10-LABX-0039-PALM) and by the ANR "Iridoti" (Grant ANR-13-IS04-0001). The work of L.K.-E. was supported by the funds from NSF DMR-1312483 (MWN), DMR -1420634 (MRSEC), NSF HRD-1547830 (CREST) and DOD W911NF-13-1-0159. Finally, the work of A.W. was partially supported by the National Science Centre, Poland, grant no UMO-2016/21/B/ST3/02565.

Appendix A: Charge Transport in thick BTS Single Crystals.

Figs. 8(a) and 8(b) show the measured Hall coefficient, R_H, and resistivity, ρ, from pristine BTS and Sn-doped single crystals. Spark-welded contacts were placed on the corners in van der Pauw configuration. One can see that high resistivity is achieved at low temperatures that is an indication of an insulating behavior. Figure 8(c) shows the Arrhenius plot of ρ. The measured magnetoresistivity, ρ_{xy}, from a 80 μm thick BTS S1 single crystals as a function of the magnetic field H_z at various angles with respect to the c-axis is given in Fig. 8(d). The weak antilocalization "cusp" is independent of the magnetic field tilt angle, and hence has a two-dimensional (involving surface and subsurface) character, even in such thick crystals.

Appendix B: Fluence and Temperature Dependence of the Surface Photovoltage.

The evolution of the SPV as a function of the incident pump fluence, P, for both pristine compounds BTS S1 and S2 were obtained by integrating energy distribution curves near $\bar{\Gamma}$ acquired at various photo-excitation fluencies at Δt=4 μs−2 ps. The results are shown in Fig. 9. Beyond a certain fluence, both SPV = $f(P)$

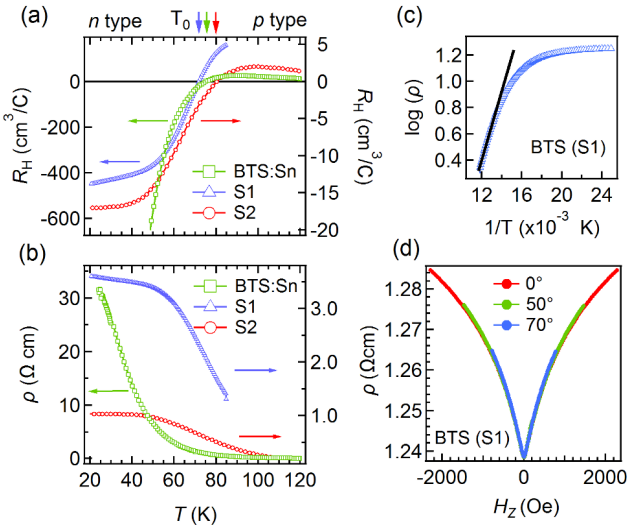

FIG. 8. (Color online) (a) Hall coefficient $R_{\rm H}$ and (b) resistivity ρ as a function of temperature T of ~ 80 μm thick and $\sim 1\times1$ mm^2 area of two pristine Bi_2Te_2Se single crystals labeled as S1 (blue curves) and S2 (red curves), and a Sn-doped Bi_2Te_2Se (green curves). At low temperatures (below $T_0 \simeq$ 73-80 K) all specimens are n-type (electron conductors). At high temperatures the conduction is p-type reflecting thermal activation of bulk hole carriers above T_0. (c) The Arrhenius fit for $T > T_0$. (d) Angle-dependent magnetoresistivity, ρ, at 8 K as a function of the applied magnetic field, H_z=H cos(ϕ).

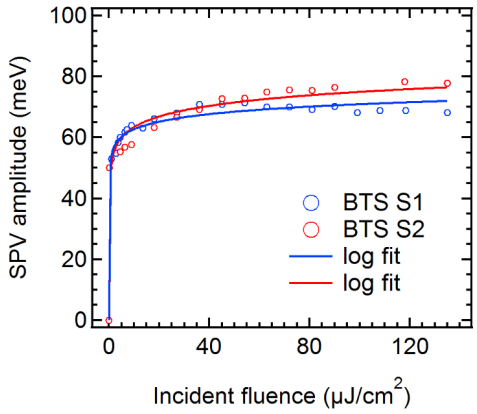

FIG. 9. (Color online) Measured SPV amplitude as a function of pump fluence for both stoichiometric BTS specimens S1 (blue dots) and S2 (red dots). The energy shifts have been measured at a constant pump-probe delay of 4 μs$-$2 ps at 40 K. Blue and red lines are logarithmic fits to the data.

curves reach saturation. In principle, a sufficiently intense illumination should flatten the surface band bending, and therefore, the photosaturation regime should be achieved. Nevertheless, it is known that under a certain illumination intensity the absolute value of the SPV is expected to diminish due to Dember effect[43]. SPV $= f(P)$ curves follow the logarithmic equation[44]:

$$\mathrm{SPV}(P) = \alpha kT \ln(1 + P/S), \tag{B1}$$

where α is equivalent to the ideality factor in a Schottky diode ($0.5 < \alpha < 2$) and S is a proportionality constant. The results show, on one hand, that the employed photoexcitation fluences set the observed SPV maximum amplitude in the saturation regime. On the other hand, the ideality factors were retrieved from fits (for specimen S1, $\alpha = 0.86 \pm 0.06$ and S2, $\alpha = 1.34 \pm 0.1$) suggest that surface trapping of excess carriers is likely present in specimen S1.

The thickness of the depletion layer, w, has been computed using the following equation:

$$w = \sqrt{\frac{2\epsilon\epsilon_0 V}{e n_{\rm B}}}, \tag{B2}$$

where ϵ is the static dielectric constant, ϵ_0 is the vacuum permittivity, V is the surface barrier height, e is the electron charge, $n_{\rm B}$ is the bulk carrier concentration at a certain temperature. At 40 K, BTS S1 specimen possesses $n_{\rm B} \sim 1.5 \times 10^{17}$ cm^{-3}, $V \sim 0.08$ V and $\epsilon \approx 95$ obtained from Akrap *et al.*[45]. Therefore, this suggests a depletion depth of ≈75 nm.

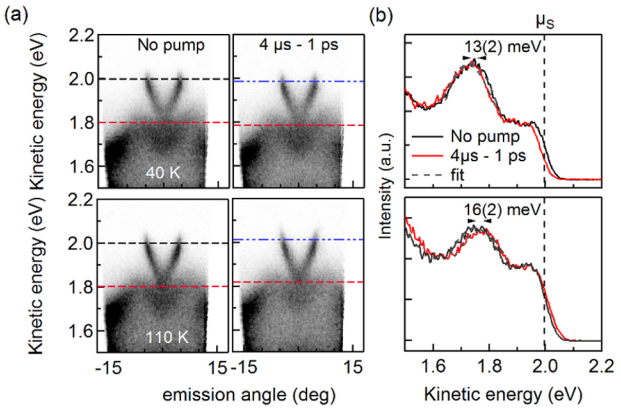

FIG. 10. (Color online) (a) ARPES intensity maps with and without pump for temperatures above and below T_0. (b) Angle-integrated intensity maps around $\bar{\Gamma}$. The SPV amplitude reaches ≈16 meV.

Figure 10 shows the evolution of the SPV as a function of temperature for a Sn-doped BTS compound. The highest SPV amplitude recorded is nearly 16 meV. We can further speculate that the Sn impurity band should have width no larger than the observed SPV.

Appendix C: Charge Transport in Exfoliated Thin BTS S1 Single Crystals.

1. Longitudinal resistivity, SdH quantum oscillations and carrier concentrations.

For 30 nm thick samples we found that the conductivity is n-type throughout the entire temperature range (see Fig. 11(a)). Table II summarizes the carrier concentration at various temperatures retrieved by assuming a SdH frequency scalling as $2\pi E_F B/(\hbar\omega)$ and a carrier concentration of $n = k_F^2/4\pi$.

TABLE II. The deduced Fermi wavevector k_F and carrier concentration n at low temperatures.

Temperature (K)	k_F (A^{-1})	n (cm^{-3})
16.7	0.0225	3.85×10^{17}
8.3	0.0318	1.08×10^{18}

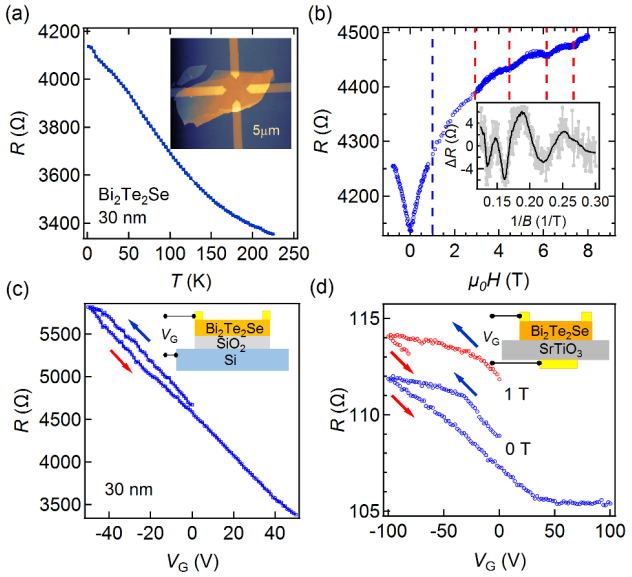

FIG. 11. (Color online) (a) Longitudinal sheet resistance R of a 30 nm thick BTS crystal. The resistance is thermally activated (non-metallic) and high. Inset: AFM image of the sample showing contacts in the van der Pauw configuration. (b) Measured R showing weak antilocalization cusp (WAL)[46] at low fields characteristic to TIs[8,9] and SdH quantum oscillations at high fields. The inset shows the SdH oscillations after background subtraction. The black curve is guide to the eye. (c) Longitudinal resistance of the sample in (a) as a function of the back-gate voltage V_G at 1.9 K. Here gate dielectric is a 90 nm thick SiO_2. A non-negligible hysteresis is visible. (d) Hysteretic gated resistivity curves of another (750 nm thick) sample with STO used as a gate dielectric. Hysteresis persists when magnetic field is applied (here shown at 0 an 1 T) and is independent of gate dielectric.

We also found that the carrier concentration in the thinner samples is much higher than in the thicker samples and that the surface carrier mobility is low (less than 100 cm^2/Vs) albeit inline with previous reports[40] in thin samples[47]. The low surface carrier mobility was previously attributed to be due to strong electron-phonon scattering[48]. Carrier densities determined from SdH quantum oscillations at 1.9 K in the thinner samples were found to be lower than from Hall resistivity (see Fig. 11). This may indicate that Hall effect detects the contribution mainly from the bulk or impurity states.

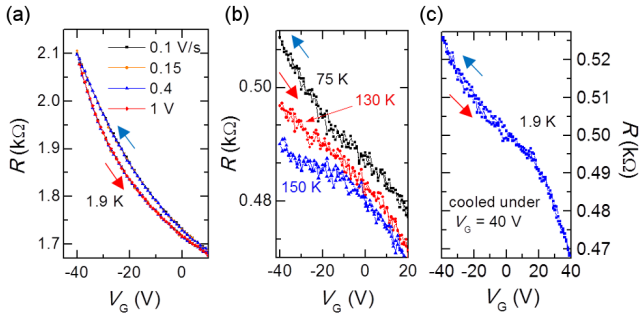

FIG. 12. (Color online) Gating hysteresis in the longitudinal sheet resistance, R, of a 30 nm thick pristine BTS single crystal flake measured at various back-gate voltage V_G sweep rates. (a) Hysteresis appears to be independent of rate in the 0.1 to 1 V/s range. Moreover, hysteresis vanishes (b) at high temperatures and (c) when the crystal is cooled to lowest temperatures under hight positive V_G.

2. Electrostatic gate-dependent charge transport in thin crystals.

The transport characteristics of the BTS devices were measured from 300 K down to 1.9 K. Figs. 11(c) and 11(d) show the measured sheet resistance, R, from a 30 nm thick and from 750 nm thick single crystal flakes as a function of the back-gate voltage V_G. The counter-clockwise gating hysteresis loop ΔR vs. V_G of a p-type (hole-conducting) BTS at low temperatures can be understood as a gradual population/depopulation of net charge between the gate and the surface 2D hole gas (2DHG). Forward gate bias sweep shifts negative charge toward the gate, resulting in the increased carrier density in the channel. Adding negative charge to the gate produces net positive charge accumulation, and eventually (as the Fermi level is moved deeper down into valence band) the accumulation can be brought to a stop producing a plateau in the $R(V_G)$, as we observe for $V_G \geq 50$ V (see Fig. 11(d)). By reversing gate bias (on the 'down-sweep') negative charge is removed from the gate, leading to repopulation of 2DHG and the reduction of the accumulated net positive charge. If negative charge is trapped by the SSs, the reduction could be very slow and the hysteresis is obtained. This behavior is well known in e.g. p-type AlGaAs/GaAs heterostructures[41], and in III-V[49]

and organic semiconductor[50] FETs. Our experiments using different gate dielectrics of various thicknesses (*i.e.* 90 nm SiO2 and up to 100 μm STO), where hysteresis $\Delta R/R{\sim}1\%$ is nearly the same for the thick and thin BTS films, exclude gate leakage as a source of hysteresis. At higher temperatures above T_0 (Fig. 12(b)), BTS turns n-type which in heterostructures has been known to be less hysteretic[41], and thermal detrapping further reduces or eliminates the hysteretic gate. Finally, hysteresis can be removed by cooling under high $V_{\rm G}$ (Fig. 12(c)) suggesting that trap states and thus carrier relaxation rates could potentially be manipulated by gate voltage.

* Corresponding author: evangelos.papalazarou@u-psud.fr

[1] M Z Hasan and C. L. Kane, "Colloquium : Topological insulators," Rev. Mod. Phys. **82**, 3045–3065 (2010).

[2] Xiao-Liang Qi and Shou-Cheng Zhang, "opological insulators and superconductors," Rev. Mod. Phys. **83**, 1057 (2011).

[3] Oleg Yazyev, Joel Moore, and Steven Louie, "Spin Polarization and Transport of Surface States in the Topological Insulators Bi_2Se_3 and Bi_2Te_3 from First Principles," Phys. Rev. Lett. **105**, 266806 (2010).

[4] L. Fu and E. Berg, "Odd-Parity Topological Superconductors: Theory And Application To $Cu_xBi_2Se_3$," Phys. Rev. Lett. **105**, 045302 (2010).

[5] S. Xu, N. Alidoust, I. Belopolski, A. Richardella, C. Liu, M. Neupane, G. Bian, S. Huang, R. Sankar, C. Fang, B. Dellabetta, W. Dai, Q. Li, M. Gilbert, F. Chou, N. Samarth, and M. Hasan, "Momentum-space imaging of Cooper pairing in a half-Dirac-gas topological superconductor," Nature Physics **10**, 943–950 (2014).

[6] Y L Chen, J. G. Analytis, J.-H. Chu, Z. K. Liu, S Mo, X. L. Qi, J Zhang, D H Lu, X Dai, Z Fang, S. C. Zhang, I R Fisher, Z. Hussain, and Z-X Shen, "Experimental Realization of a Three Dimensional Topological Insulator, Bi$_2$Te$_3$," Science **325**, 178–181 (2009).

[7] D Hsieh, Y Xia, D Qian, L Wray, J H Dil, F Meier, J Osterwalder, L Patthey, J G Checkelsky, N P Ong, a V Fedorov, H Lin, a Bansil, D Grauer, Y S Hor, R J Cava, and M Z Hasan, "A tunable topological insulator in the spin helical Dirac transport regime." Nature **460**, 1101–5 (2009).

[8] L. Zhao, M. Konczykowski, H. Deng, I. Korzhovska, M. Begliarbekov, Z. Chen, E. Papalazarou, M. Marsi, L. Perfetti, A. Hruban, A. Wołoś, and L. Krusin-Elbaum, "Stable topological insulators achieved using high energy electron beams," Nature Communications **7**, 10957 (2016).

[9] Z. Chen, L. Zhao, K. Park, T. A. Garcia, M. C. Tamargo, and L. Krusin-Elbaum, "Robust topological interfaces and charge transfer in epitaxial Bi_2Se_3/II-VI semiconductor superlattices," Nano Letters **15**, 6365 (2015).

[10] J. A. Sobota, S. Yang, J. G. Analytis, Y. L. Chen, I. R. Fisher, P. S. Kirchmann, and Z.-X. Shen, "Ultrafast Optical Excitation of a Persistent Surface-State Population in the Topological Insulator Bi_2Se_3," Phys. Rev. Lett. **108**, 117403 (2012).

[11] J. A. Sobota, S.-L. Yang, A. F. Kemper, J. J. Lee, F. T. Schmitt, W. Li, R. G. Moore, J. G. Analytis, I. R. Fisher, P. S. Kirchmann, T. P. Devereaux, and Z.-X. Shen, "Direct Optical Coupling to an Unoccupied Dirac Surface State in the Topological Insulator Bi_2Se_3," Phys. Rev. Lett. **111**, 1368 (2013).

[12] Y. H. Wang, D. Hsieh, E. J. Sie, H. Steinberg, D. R. Gardner, Y. S. Lee, P. Jarillo-Herrero, and N. Gedik, "Measurement of intrinsic Dirac fermion cooling on the surface of a topological insulator Bi_2Se_3 using time- and angle-resolved photoemission spectroscopy," Phys. Rev. Lett. **109**, 127401 (2012).

[13] A Crepaldi, B Ressel, F Cilento, M Zacchigna, C Grazioli, H Berger, Ph Bugnon, K Kern, M Grioni, and F Parmigiani, "Ultrafast photodoping and effective Fermi-Dirac distribution of the Dirac particles in Bi_2Se_3," Phys. Rev. B **86**, 205133 (2012).

[14] A. Crepaldi, F. Cilento, B. Ressel, C. Cacho, J. C. Johannsen, M. Zacchigna, H. Berger, Ph. Bugnon, C. Grazioli, I. C. E. Turcu, E. Springate, K. Kern, M. Grioni, and F. Parmigiani, "Evidence of reduced surface electron-phonon scattering in the conduction band of Bi_2Se_3 by nonequilibrium ARPES," Phys. Rev. B **88**, 121404 (2013).

[15] M Hajlaoui, E Papalazarou, J Mauchain, G Lantz, N Moisan, D Boschetto, Z Jiang, I Miotkowski, Y P Chen, A Taleb-Ibrahimi, L Perfetti, and M Marsi, "Ultrafast surface carrier dynamics in the topological insulator Bi_2Te_3." Nano Letters **12**, 3532 (2012).

[16] M Hajlaoui, E Papalazarou, J Mauchain, L Perfetti, a Taleb-Ibrahimi, F Navarin, M Monteverde, P Auban-Senzier, C.R. Pasquier, N Moisan, D Boschetto, M Neupane, M.Z. Hasan, T Durakiewicz, Z Jiang, Y Xu, I Miotkowski, Y.P. Chen, S Jia, H.W. Ji, R.J. Cava, and M Marsi, "Tuning a Schottky barrier in a photoexcited topological insulator with transient Dirac cone electron-hole asymmetry," Nature Communications **5**, 3003 (2014).

[17] Madhab Neupane, Su-Yang Xu, Yukiaki Ishida, Shuang Jia, Benjamin M Fregoso, Chang Liu, Ilya Belopolski, Guang Bian, Nasser Alidoust, Tomasz Durakiewicz, Victor Galitski, Shik Shin, Robert J. Cava, and M. Zahid Hasan, "Gigantic surface life-time of an intrinsic topological insulator," Phys. Rev. Lett. **115**, 116801 (2015).

[18] A. Sterzi, G. Manzoni, L. Sbuelz, F. Cilento, M. Zacchigna, Ph. Bugnon, A. Magrez, H. Berger, A. Crepaldi, and F. Parmigiani, "Bulk diffusive relaxation mechanisms in optically excited topological insulators," Phys. Rev. B **95**, 115431 (2017).

[19] Y Ishida, T Otsu, T Shimada, M Okawa, Y Kobayashi, F Iga, Y Takabatake, and S Shin, "Emergent photovoltage on SmB_6 surface upon bulk-gap evolution revealed by pump-and-probe photoemission spectroscopy," Sci. Rep. **5**, 1–6 (2015).

[20] Zhi Ren, A. A. Taskin, Satoshi Sasaki, Kouji Segawa, and Yoichi Ando, "Large bulk resistivity and surface quantum oscillations in the topological insulator Bi_2Te_2Se," Phys. Rev. B **82**, 241306 (2010).

[21] M. Nurmamat, E. E. Krasovskii, K. Kuroda, M. Ye, K. Miyamoto, M. M. Nakatake, T. Okuda, H. Namatame, M. Taniguchi, E. V. Chulkov, K. A. Kokh, O. E. Tereshchenko, and A. Kimura, "Unoccupied topological surface state in Bi_2Te_2Se," Phys. Rev. B **88**, 081301(R) (2013).

[22] D. O. Scanlon, P. D C King, R. P. Singh, A. De La Torre, S. McKeown Walker, G. Balakrishnan, F. Baumberger, and C. R A Catlow, "Controlling bulk conductivity in topological insulators: Key role of anti-site defects," Advanced Materials **24**, 2154–2158 (2012).

[23] S. Kushwaha, Q. Gibson, J. Xiong, I. Pletikosic, A. Weber, A. Fedorov, N. Ong, T. Valla, and R. Cava, "Comparison Of Sn-Doped And Nonstoichiometric Vertical-Bridgman-Grown Crystals Of The Topological Insulator Bi_2Te_2Se," Journal of Applied Physics **115**, 143708 (2014).

[24] J. Faure, J. Mauchain, E. Papalazarou, W. Yan, J. Pinon, M. Marsi, and L. Perfetti, "Full characterization and optimization of a femtosecond ultraviolet laser source for time and angle-resolved photoemission on solid surfaces," Review of Scientific Instruments **83**, 043109 (2012).

[25] M. Alonso, R. Cimino, and K. Horn, "Surface Photovoltage Effects In Photoemission From Metal-Gap(110) Interfaces: Importance For Band Bending Evaluation," Phys. Rev. Lett. **64**, 1947–1950 (1990).

[26] K. Horn, M. Alonso, and R. Cimino, "Non-Equilibrium Effects In Photoemission From Metal-Semiconductor Interfaces," Applied Surface Science **56–58**, 271–289 (1992).

[27] M. Marsi, L. Nahon, M. Couprie, D. Garzella, T. Hara, R. Bakker, M. Billardon, A. Delboulbé, G. Indlekofer, and A. Taleb-Ibrahimi, "Surface Photovoltage In Semiconductors Under Pulsed Optical Excitation, And Its Relevance To Synchrotron Radiation Spectroscopy," Journal of Electron Spectroscopy and Related Phenomena **94**, 149–157 (1998).

[28] L Rettig, P S Kirchmann, and U Bovensiepen, "Ultrafast dynamics of occupied quantum well states in Pb/Si(111)," New J. Phys. **14**, 023047 (2012).

[29] H. Lüth, *Solid Surfaces, Interfaces And Thin Films* (Springer Berlin Heidelberg, 2010).

[30] Jun Xiong, Yongkang Luo, YueHaw Khoo, Shuang Jia, R. J. Cava, and N. P. Ong, "High-field Shubnikov–de Haas oscillations in the topological insulator Bi_2Te_2Se," Phys. Rev. B **86**, 045314 (2012).

[31] Jun Xiong, A C Petersen, Dongxia Qu, Y S Hor, R J Cava, and N P Ong, "Quantum oscillations in a topological insulator Bi_2Te_2Se with large bulk resistivity (6 Ohm cm)," Physica E **44**, 917–920 (2012).

[32] Jun Xiong, Yuehaw Khoo, Shuang Jia, R. J. Cava, and N. P. Ong, "Tuning the quantum oscillations of surface Dirac electrons in the topological insulator Bi_2Te_2Se by liquid gating," Phys. Rev. B **88**, 035128 (2013).

[33] B.I. Shklovskiĭ and A.L. Ėfros, *Electronic Properties of Doped Semiconductors* (Springer-Verlag Berlin Heidelberg, 1984).

[34] Jens Christian Johannsen, Søren Ulstrup, Alberto Crepaldi, Federico Cilento, Michele Zacchigna, Jill A Miwa, Cephise Cacho, Richard T Chapman, Emma Springate, Felix Fromm, Christian Raidel, Thomas Seyller, Phil D C King, Fulvio Parmigiani, Marco Grioni, and Philip Hofmann, "Tunable Carrier Multiplication and Cooling in Graphene," Nano Lett. **15**, 326–331 (2015).

[35] M. K. Fuccillo, Shuang Jia, M. E. Charles, and R. J. Cava, "Thermoelectric properties of Bi2Te2Se compensated by native defects and Sn doping," J. Electron. Mater. **42**, 1246–1253 (2013).

[36] J Sanchez-Barriga, M Battiato, E Golias, A Varykhalov, L V Yashina, and O Kornilov, "at room temperature Laser-induced persistent photovoltage on the surface of a ternary topological insulator at room temperature," Appl. Phys. Lett. **110**, 141605 (2017).

[37] Kyungwha Park, Christophe De Beule, and Bart Partoens, "The ageing effect in topological insulators : evolution of the surface electronic structure of Bi_2Te_2Se upon K adsorption The ageing effect in topological insulators : evolution of the surface electronic structure of Bi_2Te_2Se upon K adsorption," New J. Phys. **15**, 16 (2013).

[38] Tobias Förster, Peter Krüger, and Michael Rohlfing, "Ab initio studies of adatom- and vacancy-induced band bending in Bi$_2$Se$_3$," Phys. Rev. B **91**, 035313 (2015).

[39] Xiaodong Xu, Wang Yao, Di Xiao, and Tony F. Heinz, "Spin and pseudospins in layered transition metal dichalcogenides," Nat. Phys. **10**, 343–350 (2014).

[40] Z. Ren, A. A. Taskin, S. Sasaki, K. Segawa, and Y. Ando, "Fermi level tuning and a large activation gap achieved in the topological insulator Bi_2Te_2Se by Sn doping," Phys. Rev. B **85**, 155301 (2012).

[41] A. Burke, D. Waddington, D. Carrad, R. Lyttleton, H. Tan, P. Reece, O. Klochan, A. Hamilton, A. Rai, D. Reuter, Wieck A., and A. Micolich, "Origin Of Gate Hysteresis In P-Type Si-Doped Algaas/Gaas Heterostructures," Phys. Rev. B **86**, 165309 (2012).

[42] B. Seradjeh, J. E. Moore, and M. Franz, "Exciton condensation and charge fractionalization in a topological insulator film," Phys. Rev. Lett. **103** (2009), 10.1109/TED.2010.2059029.

[43] Leeor Kronik and Yoram Shapira, "Surface photovoltage phenomena : theory , experiment , and applications," Surf. Sci. **37**, 1–206 (1999).

[44] B. I. Bednyi and N. V. Baidus, "Effect of recombination in the space charge region on the illuminance characteristics of the surface photo-emf of GaAs and InP," Semiconductors **27**, 620–622 (1993).

[45] Ana Akrap, Michaël Tran, Alberto Ubaldini, Jérémie Teyssier, Enrico Giannini, Dirk van der Marel, Philippe Lerch, and Christopher C. Homes, "Optical properties of Bi$_2$Te$_2$Se at ambient and high pressures," Phys. Rev. B **86**, 235207 (2012).

[46] G. Bergmann, "Weak localization in thin films: a time-of-flight experiment with conduction electrons," Physics Reports **107**, 1–58 (1984).

[47] Yong Seung Kim, Matthew Brahlek, Namrata Bansal, Eliav Edrey, Gary A. Kapilevich, Keiko Iida, Makoto Tanimura, Yoichi Horibe, Sang-Wook Cheong, and Seongshik Oh, "Thickness-dependent bulk properties and weak antilocalization effect in topological insulator bi_2se_3," Phys. Rev. B **84**, 073109 (2011).

[48] S. Giraud, A. Kundu, and R. Egger, "Electron-phonon scattering in topological insulator thin films," Phys. Rev. B **85**, 035441 (2012).

[49] M. Sonnet, C. L. Hinkle, D. Heh, G. Bersuker, and E. M. Vogel, "Impact of Semiconductor and Interface-State Capacitance on Metal/High-k/GaAs Capacitance–Voltage Characteristics," IEEE Transactions on Electron Devices **57** (2010), 10.1109/TED.2010.2059029.

[50] M. E. Gershenson, V. Podzorov, and A. F. Morpurgo, "Colloquium: Electronic transport in single-crystal organic transistors," Rev. Mod. Phys. **78**, 973–989 (2006).